Spontaneous magnetization in homometallic μ_6-oxalate coordination polymers

M. Nieves Corella-Ochoa,[a] Jordi Benet-Buchholz,[a] Marta Martínez-Belmonte,[a] and José Ramón Galán-Mascarós*[a,b]

[a]Institute of Chemical Research of Catalonia (ICIQ), Av. Països Catalans 16, 43007 Tarragona, Spain

[b]Catalan Institute of Research and Advanced Studies (ICREA), Passeig Lluïs Companys 23, 08010 Barcelona, Spain

ABSTRACT: Reaction of 1,2,4-triazole and NaF with M(ox) (M = transition metal dication; ox = oxalate dianion) under hydrothermal conditions has lead to the isolation of a variety of hybrid organic-inorganic coordination polymers. Four structurally different 3D networks were obtained, depending on the transition metal, with stoichiometry: $[M_2(H_2O)(\mu_2\text{-ox})][M_2(\mu_3\text{-trz})_6]$ (M = Fe (**1**), Co(**2**), Ni (**3**)), $[Zn_2(H_2O)(\mu_3\text{-trz})_2(\mu_2\text{-ox})]$ (**4**), $[Mn_3(\mu_3\text{-trz})_2(\mu_6\text{-ox})(\mu_3\text{-F})_2]$ (**5**) and $[Fe_3(\mu_3\text{-trz})_2(\mu_6\text{-ox})(\mu_2\text{-F})_2]$ (**6**). In all cases, the magnetic behavior is dominated by antiferromagnetic exchange interactions between paramagnetic centers. Remarkably, **5** and **6** present a novel magnetic connectivity around the oxalate anion: a μ_6-bridging mode. This magnetic geometry promotes multiple triangular arrangements among antiferromagnetically coupled spin carriers resulting in a complex magnetic network due to the presence of competing interactions. These materials exhibit spontaneous magnetization below 9 and 66 K, respectively.

INTRODUCTION

Over the past decades organic-inorganic hybrid coordination polymers have occupied a prominent position in the field of materials science due to their wide range of technological applications.[1–5] The design tools are well established and involve the use of connectors (inorganic units, metal complexes) and linkers (organic molecules) as the main building units. Both parts play a crucial role in the functionality of the final structure. In the field of magnetic materials, molecule-based magnets[6] have successfully reached features usually associated with classic inorganic solids, such as high ordering temperatures[7-10] or large magnetic hysteresis.[11-12] These unique materials possess, at the same time, properties typically associated with molecules: light-weighted, transparent, easily processable, etc.

The design of molecule-based magnets requires the use of linkers able to promote strong super-exchange interactions when high temperature magnetic phenomena are desired. This means short bridges between spin carriers are mandatory. Single-atom bridges, such as oxo or fluoride, promote very strong coupling.[13] However, it is synthetically difficult to incorporate such highly electronegative connectors maintaining a molecular character, since they favor the formation of ionic solid state compounds.

The most successful ligands in the search for molecule-based magnets have been short (two or three atoms) bridges with an efficient π pathway such as cyanide,[14-18] carboxylate,[19] oxalate,[20-25] azide,[26-29] or dicyanamide.[14,30-34] These organic ligands promote ferromagnetic (FM) or antiferromagnetic (AF) exchange interactions depending on their connecting modes. FM interactions are typically weak, whereas AF interactions can be very strong resulting in high temperature magnetic phenomena. However, AF coupling typically stabilizes a non-magnetic ground state in homometallic compounds, due to the alternating orientation of identical spins. To take advantage of these strong AF interactions, heterometallic compounds or organic radicals linkers[35] have been used to yield high temperature ferrimagnets. Homospin systems, where the AF interactions are maximized because of the perfect energy matching between atomic orbitals, need the appearance of spin canting between antiparalleled magnetic moments to yield weak ferromagnets.[36-38] Spin canting depends on small deviations from perfect alignment between local magnetic moments due to geometrical or electronic anisotropy.[39]

The electronic origin for canted alignment of spins can arise from single-ion anisotropy and/or antisymmetric spin–spin coupling (termed as the Dzyaloshinski–Moriya interaction). Geometrical anisotropy appears when the crystal lattice is incompatible with AF dominant interactions. This is the case, for example, in a triangular array of AF coupled metal centers. This geometry promotes competing AF interactions[40] and stabilization of a magnetic ground state.[41,42] The appearance of spontaneous magnetization in strongly AF coupled homospin systems keeps attracting interest as a plausible strategy to reach high ordering temperatures.[43,44] The best examples have appeared in oxo-centered triangular arrays.[45]

The multidentate oxalate (ox) ligand (Figure 1) is the shortest organic ligand with more coordination modes able to induce triangular arrangements when it connects more than

two centers (Figure 1). However, the main connecting mode with transition metals is the μ_2-bis-chelating (Figure 1a), being higher connectivity rare.[23] The most promising mode for the development of magnetic materials is the μ_6 (Figure 1d), since it should promote competing interactions arising from the multiple triangular arrangements, but to date, it has only been reported with diamagnetic alkali metal ions.

Here we report multicomponent reactions by combining oxalate, 1,2,4-trizolate and fluoride ligands with divalent metal centers. We have been able to isolate six novel compounds under hydrothermal conditions, belonging to four structural motifs: $[M_2(H_2O)(\mu_2\text{-ox})][M_2(\mu_3\text{-trz})_6]$ (M = Fe (**1**), Co(**2**), Ni (**3**)), $[Zn_2(H_2O)(\mu_3\text{-trz})_2(\mu_2\text{-ox})]$ (**4**), $[Mn_3(\mu_3\text{-trz})_2(\mu_6\text{-ox})(\mu_3\text{-F})_2]$ (**5**) and $[Fe_3(\mu_3\text{-trz})_2(\mu_6\text{-ox})(\mu_2\text{-F})_2]$ (**6**). These materials represent a new family of oxalate-based coordination polymers with unprecedented architectures. Remarkably, the elusive μ_6-oxalate bridging mode has been found in compounds **5** and **6**, which induces competing interactions and the appearance of spontaneous magnetization.

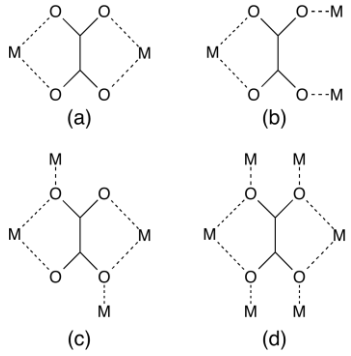

Figure 1. Bridging coordination modes of oxalate anion with transition metal cations (M). (a) μ-bridging mode. (b) μ_3-bridging mode. (c) μ_4-bridging mode. (**d)** μ_6-bridging mode, unprecedented for six paramagnetic transition metal centers.

EXPERIMENTAL

All reagents and chemicals were supplied by Sigma Aldrich Chemical Company Ltd. and Across Organics. Unless stated otherwise, the materials were used without further purification. Elemental analyses (C, H, N and F) were carried out by iQAC Servei de Microanàlisis (CSIC, Barcelona). FT-IR spectra were collected in transmission mode using a Bruker Optics FT-IR Alpha spectrometer in the 4000-400 cm^{-1} range. Thermogravimetric analyses were performed with a TGA/SDTA851 Mettler Toledo under nitrogen flow at a heating rate of 10 °C min^{-1}. Powder X-ray diffraction (PXRD) data was collected on a D8 Advance series 2Theta/Theta powder diffractometer at room temperature. Magnetic susceptibility measurements between 2-300 K were carried out in a Quantum Design MPMS-XL SQUID magnetometer using a 1000 Oe field. Pascal's constants were used to estimate the diamagnetic corrections for the compounds. Data for compound **1** showed a paramagnetic impurity that was also corrected, accounting for 2.5 % of the total signal. Zero field cooled, field cooled and remnant magnetization measurements were carried out using a 25 Oe field. Magnetization curves were collected between –7 and 7 T at 2 and 10 K.

Synthesis of $[Fe_2(H_2O)(C_2O_4)][Fe_2(C_2H_2N_3)_6]\cdot 2.5H_2O$ (1). A mixture of $Fe(ox)\cdot 2H_2O$ (0.22 g, 1.5 mmol), 1,2,4-triazole (0.42 g, 6 mmol), NaF (50 mg) and water (10 mL) was heated at 180 ºC for a week under autogenous pressure. The mixture was cooled to room temperature. Brown prism-shaped crystals from **1**, suitable for X-ray structure analysis, were obtained. Yield 165.1 mg, 56% (based on Fe). Elemental analysis for $C_{14}H_{19}Fe_4N_{18}O_{7.5}$ (782.80); calc: C: 21.48 %, H: 2.45 %, N: 32.21 %; found: C: 21.25 %, H: 1.91 %, N: 31.93 %. FT-IR (cm^{-1}): 1637 s, 1488 s, 1281 s, 1145 s, 986 s, 665 s, 620 s.

Synthesis of $[Co_2(H_2O)(C_2O_4)][Co_2(C_2H_2N_3)_6]\cdot 4H_2O$ (2). A mixture of $Co(ox)\cdot 2H_2O$ (0.1 g, 0.55 mmol), 1,2,4-triazole (0.1 g, 1.45 mmol), NaF (50 mg) and water (10 mL) was heated at 180 ºC for a week under autogenous pressure. The mixture was cooled to room temperature. A pink solid of **2** was formed. Yield 74 mg, 65% (based on Co). Elemental analysis for $C_{14}H_{22}Co_4N_{18}O_9$ (822.17); calc: C: 20.45 %, H: 2.7 %, N: 30.67 %; found: C: 20.34 %, H: 2.45 %, N: 30.45 %. FT-IR (cm^{-1}): 1628 s, 1496 s, 1310 s, 1277 s, 1154 s, 1074 s, 993 s, 883 s, 802 s, 672 s.

Synthesis of $[Ni_2(H_2O)(C_2O_4)][Ni_2(C_2H_2N_3)_6]\cdot 4H_2O$ (3). The same procedure as for compound **2** was followed but using $Ni(ox)\cdot 2H_2O$ instead of $Co(ox)\cdot 2H_2O$. A blue solid of **3** was formed after a week under autogenous pressure. Yield 54.9 mg, 49% (based on Ni). Elemental analysis for $C_{14}H_{22}Ni_4N_{18}O_9$ (821.21); calc: C: 20.48 %, H: 2.7 %, N: 30.7 %; found: C: 20.83 %, H: 2.36 %, N: 30.44 %. FT-IR (cm^{-1}): 1631 s, 1573 s, 1499 s, 1311 s, 1281 s, 1160 s, 1083 s, 995 s, 883 s, 674 s.

Synthesis of $[Zn_2(H_2O)(C_2H_2N_3)_2(C_2O_4)]\cdot 2H_2O$ (4). A mixture of $Zn(ox)\cdot xH_2O$ (50 mg, 0.26 mmol), 1,2,4-triazole (0.109 g, 1.6 mmol), NaF (50 mg) and H_2O (10 mL) was heated at 180 ºC for a week under autogenous pressure. The mixture was cooled to room temperature. White prism-shaped crystals from **4**, suitable for X-ray structure analysis, were obtained. Yield 30.5 mg, 29% (based on Zn). Elemental analysis for $C_6H_{10}Zn_2N_6O_7$ (408.94); calc: C: 17.62 %, H: 2.46 %, N: 20.55 %; found: C: 17.88 %, H: 2.24 %, N: 20.61 %. FT-IR (cm^{-1}): 1622 s, 1512 s, 1354 s, 1308 s, 1212 s, 1154 s, 1079 s, 1005 s, 794 s, 662 s, 492s.

Synthesis of $[Mn_3(C_2H_2N_3)_2(C_2O_4)F_2]$ (5). A mixture of $Mn(ox)\cdot xH_2O$ (0.1 g, 0.7 mmol), 1,2,4-triazole (0.97 g, 1.4 mmol), NaF (50 mg) and H_2O (10 mL) was heated at 180 ºC for three days under autogenous pressure. The mixture was cooled to room temperature. Yellow crystals from **5**, suitable for X-ray structure analysis, were obtained. Yield 57 mg, 57%. Elemental analysis for $C_6H_4F_2Mn_3N_6O_4$ (426.94); calc: C: 16.88 %, H: 0.94 %, N: 19.68; found: C: 16.93 %, H: 0.94 %, N: 19.80 %. FT-IR (cm^{-1}): 1624 s, 1507 s, 1321 s, 1271 s, 1149 s, 1053 s, 993 s, 875 s, 770 s, 659 s, 513s.

Synthesis of $[Fe_3(C_2H_2N_3)_2(C_2O_4)F_2]$ (6). A mixture of $Fe(ox)\cdot 2H_2O$ (0.1 g, 0.56 mmol), 1,2,4-triazole (0.1 g, 1.45 mmol), NaF (50 mg) and water (10 mL) was heated at 180 ºC for a week under autogenous pressure. The mixture was cooled to room temperature. **1** is the main product of this reaction, with **6** being a minor product as brown hexagonal-shaped crystals. These crystals, suitable for X-ray structure analysis, were hand-collected by the Pasteur method. All characterization was carried out with single crystals.

X-ray crystallography. Single crystal X-ray diffraction measurements were made at 100 K in a Bruker APEX DUO diffractometer with a Quazar MX Multilayer Optics ($Mo_{K\alpha}$ radiation; λ = 0.71073 Å). Single crystal X-ray diffraction measurements on **1, 4**, **5** and **6** were made at 100 K using a

Bruker-Nonius diffractometer equipped with an APEX II 4K CCD area detector, a FR591 rotating anode with $Mo_{K\alpha}$ radiation (λ = 0.71073 Å) and Montel mirrors as monochromator. The structures were solved using the SIR2011 program[46] and refined on F^2 using the SHELXTL97 program.[47] Crystal data collection and refinement parameters are given in Table 1. CCDC-1033523-26 (**1**), 1033524 (**4**), 1033525 (**5**) and 1033526 (**6**) contain the supplementary crystallographic data for this paper. Compounds **2** and **3** are isostructural to **1,** as confirmed by X-ray diffraction pattern from powder samples (Figure S1). Their corresponding unit cells as estimated from the X-ray diffraction powder patterns are: **2**, monoclinic *C*2, a = 15.9229(8) Å, b = 11.0698(4) Å, c = 7.7171(5) Å, β= 90.488(5)°, V = 1360.20(11) Å^3; and **3**, monoclinic *C*2, a = 15.7272(15) Å, b = 10.9328(9) Å, c = 7.5646(8) Å, β = 90.483(9)°, V = 1300.64(22) Å^3.

RESULTS AND DISCUSSION

Synthesis

The reaction of $M(ox)\cdot 2H_2O$ (M = divalent transition metal cation; ox = oxalate dianion) and 1,2,4-triazole at 180 ºC yielded four novel compounds that can be classified into two different stoichiometries: $[M_2(H_2O)(\mu\text{-ox})][M_2(\mu_3\text{-trz})_6]$ (when M = Fe, **1**; Co, **2**; Ni, **3**) and $[Zn_2(H_2O)(\mu_3\text{-trz})_2(\mu_2\text{-ox})]$ (**4**).

Single crystals suitable for X-ray diffraction analysis of **1** and **4** were obtained by adding NaF to the reaction mixture as mineralizing agent, since the presence of fluoride anions slows the crystallization dynamics. In the case of the cobalt and nickel analogues only polycrystalline powders were isolated in all tested reaction conditions.

The presence of fluoride also allowed the isolation of two additional compounds that incorporate fluoride anions to their framework: $[M_3(\mu_3\text{-trz})_2(\mu_6\text{-ox})F_2]$ (M = Mn, **5**; Fe, **6**). **5** is the

Table 1. Crystallographic data and main refinement parameters for compounds 1, 4, 5 and 6.

Compound	1	4	5	6
Formula	$C_{14}H_{20}Fe_4N_{18}O_8$	$C_6H_{12}N_6O_8Zn_2$	$C_6H_4F_2Mn_3N_6O_4$	$C_{12}H_8F_4Fe_6N_{12}O_8$
MW	791.88	426.96	426.97	859.40
T (K)	100(2) K			
Wavelength	0.71073 Å			
Crystal system	Monoclinic			
Space group	*C*2	$P2_1/c$	$P2_1/n$	*C*2/c
a (Å)	15.653(3)	7.4835(16)	7.7577(3)	7.5869(7)
b (Å)	10.750(2)	8.8171(19)	7.2598(3)	12.6052(11)
c (Å)	7.2868(14)	10.058(2)	9.8914(4)	11.5603(10)
β (º)	90.361(6)	100.450(6)	93.941(2)	101.775(3)
V (Å^3)	1226.2(4)	652.7(2)	555.76(4)	1082.30(17)
Z	8	4	2	2
D_{calc} (g/cm^3)	2.145	2.173	2.551	2.637
Absorption coefficient (mm^{-1})	2.405	3.731	3.412	4.026
F(000)	796	428	414	840
Size (mm^3)	0.15 x 0.12 x 0.08	0.01 x 0.01 x 0.002	0.05 x 0.01 x 0.002	0.30 x 0.30 x 0.10
θ range (º)	2.30 to 25.63°	2.768 to 33.193°	3.455 to 36.366°	3.184 to 36.304°
Index ranges	$-17 \le h \le 18$ $-13 \le k \le 13$ $-8 \le l \le 8$	$-5 \le h \le 11$ $-13 \le k \le 8$ $-15 \le l \le 14$	$-12 \le h \le 10$ $-12 \le k \le 11$ $-16 \le l \le 16$	$-12 \le h \le 8$ $-20 \le k \le 20$ $-18 \le l \le 19$
Reflections collected	5928	6736	10448	7583
Independent reflections	2295	2315	2687	2440
R_{int}	0.0286	0.0358	0.0384	0.0315
Max./min. transmission	0.8309/0.7143	0.993/0.739	0.993/0.861	0.961/0.367
Data / restraints / parameters	2295 / 317 / 183	2315 / 0 / 100	2687 / 0 / 97	2440 / 258 / 153
Goodness-of-fit on F^2	1.093	1.025	1.046	1.155
R1[I>2sigma(I)]	0.0380	0.0342	0.0186	0.0320
wR2[I>2sigma(I)]	0.0881	0.0709	0.0494	0.0845
R1(all data)	0.0443	0.0512	0.0200	0.0333
wR2 (all data)	0.0923	0.0765	0.0504	0.0853
Largest diff. peak / hole (e.Å^3)	1.174/–0.823	1.534/–0.789	0.732/–0.403	2.096/–0.823

only product that was isolated with the Mn^{2+} cation, since in the absence of NaF no product was obtained. **6** is a minor product that appears when the synthesis of **1** is carried out in the presence of NaF. **6** was obtained as large and distinct single crystals reaching a maximum 5% yield by decreasing the trz ratio in the starting materials. The large size of these single crystals allowed easy hand-collection.

Structural description

$[Fe_2(H_2O)(\mu_2\text{-ox})][Fe_2(\mu_3\text{-trz})_6]\cdot\mathbf{3H_2O}$ **(1)**: It consists of a 3D coordination network with μ_2-oxalate and μ_3-triazolate bridges. Charge balance indicates all Fe centers appear in the +2 oxidation state. There are three crystallographically independent Fe positions in the structure. Fe1 is coordinated to an oxalate, a water molecule and three monodentate triazolate anions (through the N4-position). Fe2 and Fe3 are chemically equivalent, coordinated by six triazolate rings (through N1 and N2 positions). Fe2 and Fe3 build $\{Fe(trz)_3\}$ chains running along the *c* axis where the Fe^{2+} centers are connected by three triazolate bridges (Figure 2b). These 1D chains are analogous to those found in the classic triazole-based spin transition materials.[48] The intrachain Fe-Fe distance is 3.643 Å, with Fe-N distances in the 1.89-2.06 Å range, suggesting a diamagnetic low spin configuration. The propeller geometry of the triple trz bridge is staggered, with an almost perfect 60º torque angle between adjacent bridges, in such a way that the conformation is repeated every other bridge.

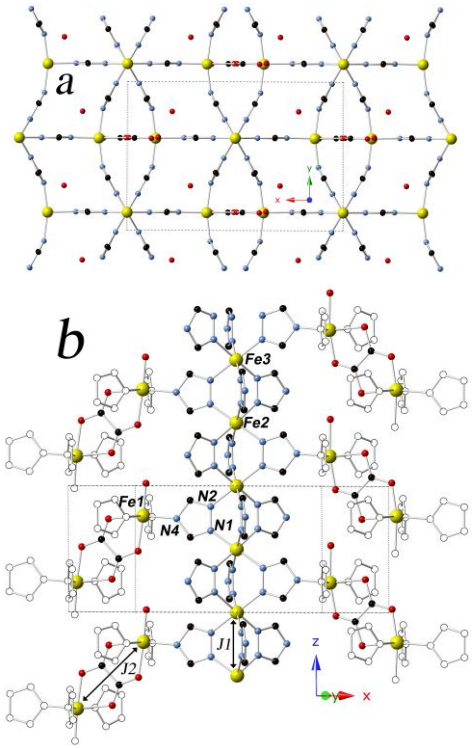

Figure 2: (a) Projection of crystal structure of **1** on the *ab* plane. (b) Representation along the *c* axis, highlighting the triply-bridged $\{Fe(trz)_3\}$ chains connected through the $[Fe_2(H_2O)(ox)]$ dimers. (color code: Fe = yellow; C = black; N = blue; O = red). Hydrogen atoms omitted for clarity.

The $\{Fe(trz)_3\}$ chains are connected to each other through the triazolate N4 position which binds to $[Fe_2(H_2O)(ox)]$ moieties *via* the Fe1 centers. Fe1 shows longer bonding distances (2.05-2.3 Å) to the chelated oxalate anion than to the three triazolate ligands shared with three adjacent chains and one water molecule (Figure 2c). This suggests high spin configuration in Fe1. Each dimer connects two adjacent chains on the *ac* plane, and two on the *bc* plane. The latter bridges are multiple, to two adjacent staggered trz bridges. Single crystals included 3 crystallization water molecules per formula unit, whereas elemental analysis and TGA in grained samples indicated slightly lower water content (2.5 water molecules per formula unit).

Compounds **2** and **3** are isostructural to **1** as confirmed by their powder X-ray diffraction patterns (Figure S1).

$[Zn_2(H_2O)(\mu_3\text{-trz})_2(\mu_2\text{-ox})]\cdot\mathbf{2H_2O}$ **(4)**: This polymeric network is built by only one crystallographic Zn site, coordinated by a chelating oxalate, three terminal trz units (through N1, N2 and N4, respectively) and a water molecule. The structure can be described as formed by chains defined by the μ-oxalate and double μ-trz bridges along the *b* axis. The N4 position, completing the μ_3-trz connectivity, links the chains to form a 3D structure (Figure 3). Additionally, there is a second water molecule making hydrogen bonds to the coordinated water molecule and to an oxalate anion.

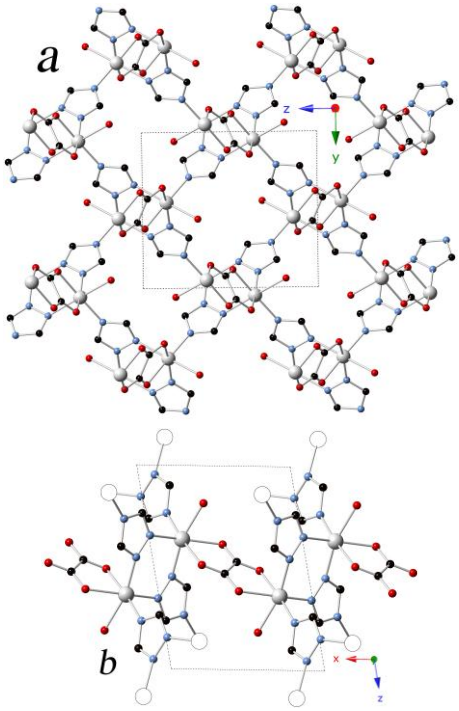

Figure 3: (a) Projection of crystal structure of **4** on the *bc* plane. (b) Representation of the doubly-bridged chains along the *b* axis. (color code: Zn = white; C = black; N = blue; O = red). Hydrogen atoms omitted for clarity.

$[Mn_3(\mu_3\text{-trz})_2(\mu_6\text{-ox})(\mu_3\text{-F})_2]$ **(5)**: There are two crystallographically independent Mn positions in this structure, in the +2 oxidation state, according to the charge balance. One is heptacoordinated (Mn1) and one hexacoordinated (Mn2). Two trz units occupy the axial positions. One chelating and one terminal oxalate units occupy the equatorial plane, opposite to each other, completed by two fluoride atoms. The oxalate bite shows significantly longer bonding distances (> 2.4 Å) than the fluoride, the terminal oxalate and the trz (in the 2.1-2.2 Å range). Mn2 shows a distorted octahedral geometry, with two fluoride atoms in the axial positions. The equatorial positions are occupied by two

monodentate oxalates and two trz in *trans* configuration. The octahedron is distorted with the axial positions significantly shorter (< 2.01 Å) than the equatorial ones (>2.18 Å).

Taking into account the magnetic connectivity, the structure can be described as formed by layers (Figure 4a), perpendicular to the *ac* plane, and defined by μ_6-oxalate, μ_3-F^- and μ_2-trz bridges. The latter are above and below the plane, where the trz ligands connect layers through its third nitrogen atom. The [Mn_3F] units form a regular triangle (Mn–F = 2.283, 2.120 and 2.091 Å). The μ_6-oxalate bridge connects four Mn1 (two chelated, two terminal) and two Mn2 centers, with a longer chelating bite (Mn–O = 2.442 and 2.491 Å), and a shorter terminal bonding (Mn–O = 2.179 and 2.276 Å).

Each metal dication is surrounded by six Mn centers, in a distorted pseudo-hexagonal array. The bridges are: a triple oxo/trz/fluoride (J1); an oxalate (J2); a double c□□□□□□□□□□□/fluoride (J3); a double o□□/fluoride (J4); and two single c□□□□□□□□□□ (J5). This creates multiple triangular arrangements, with J1/J2/J5, J4/J3/J5 and all their equivalents by symmetry. The fluoride is also at the center of a Mn triangle (Figure 4b).

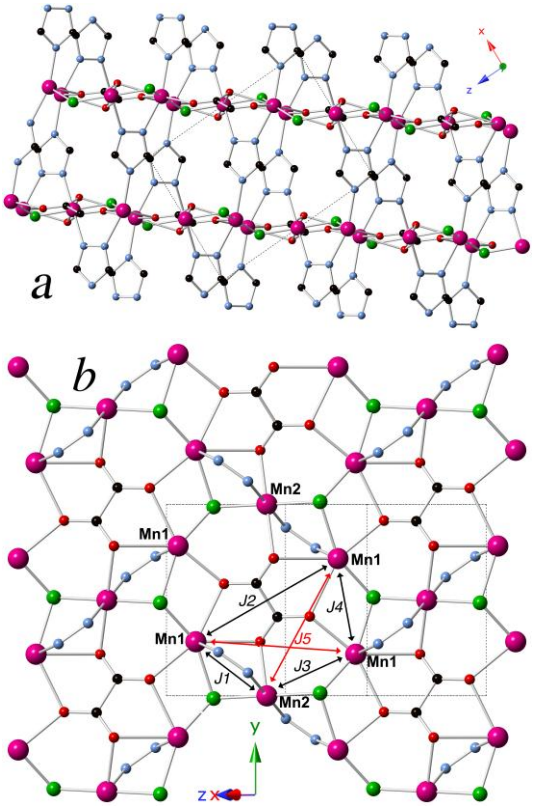

Figure 4: (a) Projection of crystal structure of **5** on the *ac* plane. (b) Representation of the multiply-bridged planes along the *b* axis, defined by the μ_6-oxalate, μ_3-F^-, and μ_2-trz bridges. (color code: Mn = pink; C = black; N = blue; O = red; F = green). Hydrogen atoms omitted for clarity.

[$Fe_3(\mu_3\text{-trz})_2(\mu_6\text{-ox})(\mu_2\text{-F})_2$] **(6)**: This structure is reminiscent of **5**, with identical stoichiometry. The main difference resides in both Fe^{2+} centers being hexacoordinated (pseudo-octahedral) and the fluoride bridges being μ_2-F^-. Fe1 is coordinated by one chelating and one monodentate oxalates, two trz (through the N1 and N4 positions) and only one fluoride. Fe2 is coordinated by two monodentate oxalate anions at the axial positions, with the equatorial positions occupied by two fluoride and two trz (N1 or N2) in *trans* configuration. In this case, the structure can be described as formed by corrugated layers parallel to the *bc* plane, defined by the μ_6-oxalate, μ_2-fluoride and triazolate bridges, with the trz ligands bridging layers as μ_3 linkers.

When compared to **5**, the μ_6-oxalate connectivity shows shorter bonds, with all six Fe–O distances in the 2.1–2.3 Å range. The shortest and longest distances belong to the oxalate chelating bite. The fluoride anion is now out of the plane defined by the metal centers, bridging Fe1 and Fe2 (Fe1–F = 1.947 and Fe2–F = 1.980 Å). The next nearest Fe atom appears at Fe–F = 2.760 Å, too long to be considered an effective bond. The magnetic connectivity in the plane is defined by an oxalate (J1); two oxo (J2,J5); two carboxylates (J3) and a double trz/fluoride (J4).

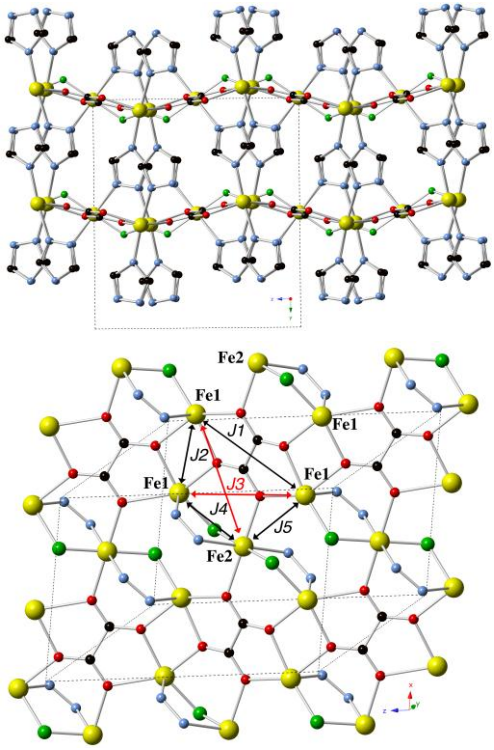

Figure 5: (a) Projection of crystal structure of **6** on the *bc* plane. (b) Representation of the multiply-bridged planes along the *a* axis, defined by the μ_6-oxalate, μ_2-F^-, and μ-trz bridges. (color code: Fe = yellow; C = black; N = blue; O = red; F = green). Hydrogen atoms omitted for clarity.

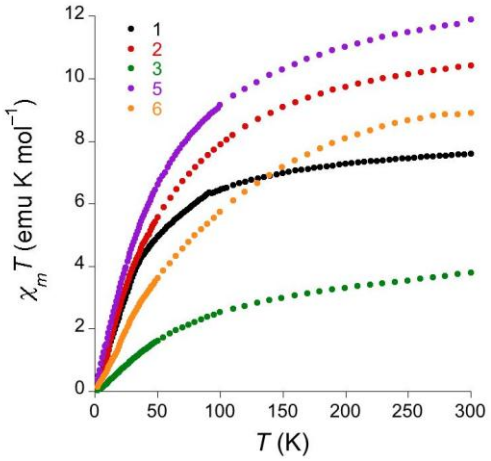

Figure 6: Thermal dependence of the χ_mT product for compounds **1**-**3**, **5** and **6** under an applied magnetic field of 1000 Oe.

Magnetic characterization

Compounds **1**-**3** are paramagnetic at room temperature with a $\chi_m T$ product of 7.60, 10.43 and 3.80 emu K mol^{-1}, respectively. This indicates high spin M^{2+} metal centers for **2** - **3**, and a mixture of low spin Fe^{2+} (S = 0 in the chain), and high spin Fe^{2+} (S = 2 in the dimer) for **1** (Table 2), as expected from the crystallographic data. As the temperature decreases, the $\chi_m T$ product (Figure 6) decreases suggesting the presence of dominant AF interactions. The high temperature regime, above 100 K, can be simulated with a Curie-Weiss law (Figure S2), yielding negative Weiss constants following the trend θ(**3**) > θ(**2**) > θ(**1**). Below 100 K, $\chi_m T$ decreases more rapidly, approaching null values at very low temperatures. The presence of dominant AF interactions is corroborated by the appearance of a maximum in χ_m (Figure 7).

In **1**, the oxalate bridge is the only effective super-exchange pathway between spin careers. Thus, the magnetic data can be modeled with an isotropic Hamiltonian for a dimer of two S centers with a J_2 coupling constant:

$$\mathrm{H} = -J_2 S_1 S_2 \tag{1}$$

Using this Hamiltonian for S = 2, the magnetic data for compound **1** can be reproduced with a weak antiferromagnetic coupling (Table 2). The S = 0 low spin configuration of the Fe centers in the chain is maintained up to 400 K. No spin transition was observed.

Since the μ_3-trz bridge should be the weakest exchange pathway when compared with the triple μ_2-trz bridges along the chain, and the bis-chelating oxalate bridge in the dimer, it can be considered negligible in a first approximation. Thus, we have modeled the magnetic data of **2** and **3** with an isotropic Hamiltonian result of the addition of a chain of n spin S centers with a J_1 superexchange parameter, plus a dimer with a J_2 parameter:

$$\mathrm{H} = -J_1 \sum_{i=1}^{n-1} S_i S_{i+1} - J_2 S_1 S_2 \tag{2}$$

Compound **2** shows a strong single ion anisotropy, typical of octahedral Co^{2+} complexes. Still, we tried to model the data with the same Hamiltonian for S = 3/2, using the analytical expression derived by Fisher for a chain:[49]

$$\chi = \frac{Ng^2\beta^2 S(S+1)}{3kT} \frac{1+u}{1-u} \tag{3}$$

with

$$u = \coth\left[\frac{JS(S+1)}{kT}\right] - \left[\frac{kT}{JS(S+1)}\right] \tag{4}$$

The best fit is surprisingly good being obtained from an isotropic model. Although the absolute numbers for J_1 and J_2 need to be taken as a rough estimation, it is interesting to note how the AF interaction in the dimer is significantly stronger, since J_2 doubles J_1.

The isotropic Hamiltonian for a chain of equally spaced isotropic S = 1 magnetic centers has an analytical expression:[50]

$$\chi = \frac{Ng^2\beta^2}{kT} \frac{2.0 + 0.0194x + 0.777x^2}{3.0 + 4.346x + 3.232x^2 + 5.834x^3} \tag{5}$$

$$\text{with } x = \frac{|J|}{kT}$$

Using this expression for **3** the fitting of the magnetic data yields a stronger overall AF exchange for this derivative, and $J_1 \approx 0.75\ J_2$ (Table 2). This is in good agreement with the exchange coupling constants found in homometallic oxalate-bridged dimers that significantly exhibited stronger coupling for Ni.[51]

Compounds **5** and **6** have a much more complex magnetic connectivity. Their magnetic data cannot be fitted to a simple model due to their layered structure with multiple and competing super-exchange pathways. The room temperature $\chi_m T$ products are 11.93 and 8.93, respectively. Both numbers are lower than the expected spin-only values (Table 2). Curie-Weiss fitting of the high temperature data yields Curie constants in good agreement with the spin only values (Table 2). The behavior of $\chi_m T$ under an applied field of 0.1 T is apparently very similar to that of the previous compounds (Figure 6). However, χ_m vs T plots are quite different. In addition to the appearance of a maximum due to the dominant AF interactions, one can observe additional features that suggest the appearance of spontaneous magnetization.

In the case of **5**, χ_m shows a maximum around 12 K, and a sudden jump below 10 K (Figure 8). The zero-field cooled (ZFC) and field cooled (FC) data show the appearance of an irreversibility (Figure 9), which suggests the onset of spontaneous magnetization. This is confirmed by the remnant magnetization (RM) that remains at zero field. RM disappears at 9.0 K, which defines the critical temperature (T_C) for this compound. Alternating current (ac) magnetic measurements (Figure S3) are significantly different from the dc data, supporting the onset of spontaneous magnetization. However, ac data are surprisingly complex. The in-phase susceptibility shows a sharp decrease below 9 K, concomitant with the appearance of a non-zero out-of-phase signal, although very weak. Even though no frequency dependence was observed. Magnetization (M) data at 2 K (Figure S4) is essentially linear up to 7 T, when it reaches 2.1 μ_B, far from the expected 15 μ_B for parallel spin alignment. This behavior is typical of magnets with dominant antiferromagnetic interactions.[52] The hysteresis loop shows memory effect, with a coercive field of 450 Oe (Figure S4).

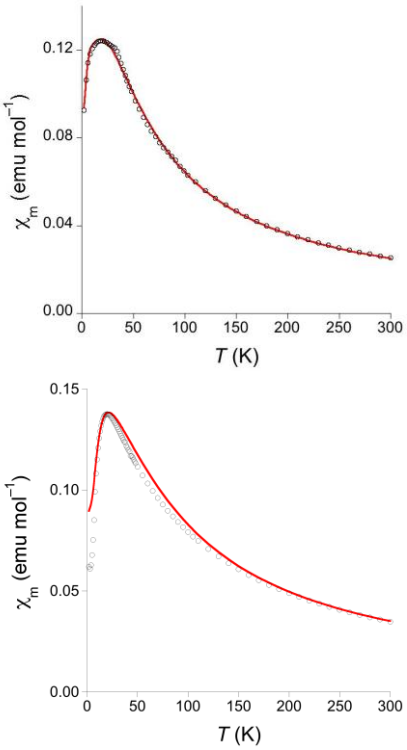

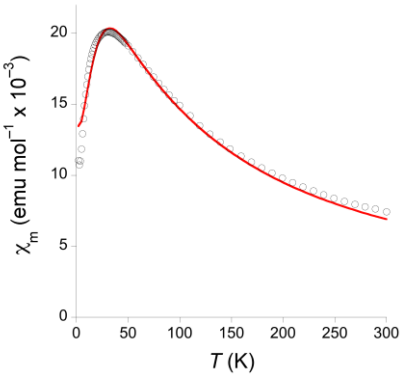

Figure 7: Thermal dependence of the magnetic susceptibility for compounds **1**, **2** and **3** respectively, measured under an applied magnetic field of 1000 Oe. Red line shows the best fitting with the model described in eq. 1.

For compound **6**, χ_m follows an apparently similar trend, reaching a round maximum at 23 K, but no jump is found below the maximum. χ_m keeps decreasing with temperature and only changes the tendency below 10 K, when it increases again (Figure 8). Surprisingly, the ZFC/FC data shows an irreversibility above 60 K (Figure 10), associated to a RM that disappears at 66 K, determining the onset of spontaneous magnetization. The ac magnetic susceptibility data shows apparently two separated processes, with two maxima in χ', associated to non-zero signal in χ'' (Figure S5). Again, the out-of-phase signal appears very weak and noisy. Multiple processes in ac data have been observed in other 2D materials and related to the low dimensionality of the magnetic networks. The assignment of these two features to multiple phases can be ruled out due to multiple (indirect) experimental evidences. The remnant magnetization of both features is comparable, both maxima are of the same magnitude and both appear in the ac and also ZFC data. Such major contribution could only arise from major contamination, which cannot exist since these measurements were carried out on grounded single crystals, hand collected, avoiding any major contamination.

Table 2. Magnetic parameters for compounds 1-3, 5 and 6.

	χT(emu K mol^{-1})[1]	XT$_{SO}$(emu K mol^{-1})	(emu K mol^{-1})		g	*J1* (cm^{-1})	*J2* (cm^{-1})	T_C (K)	H_{coer} (Oe)[2]
1	7.60	6.0	8.33	–28.9	2.30(1)	-	–5.1(2)	-	-
2	10.43	7.5	12.45	–56.5	2.50(2=	–3.1(2)	–6.2(4)	-	-
3	3.80	4.0	4.98	–98.4	2.20(2)	–12(1)	–16(2)	-	-
5	11.93	13.1	13.91	–52.2	2.1[3]	-	-	9	450
6	8.93	9.0	11.74	–90.6	2.3[3]	-	-	66	-

[1]300 K. [2]2 K. [3]Estimated from the Curie constant.

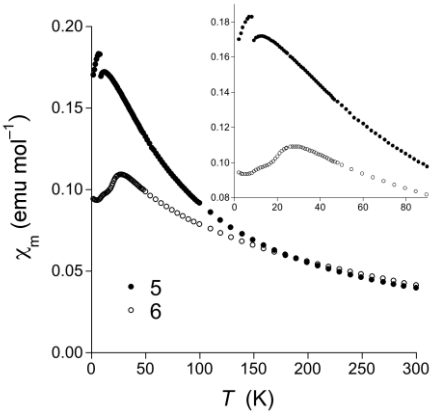

Figure 8: Thermal dependence of magnetic susceptibility for compounds **5** and **6** measured under an applied magnetic field of 1000 Oe. (inset) Detail of the low temperature data.

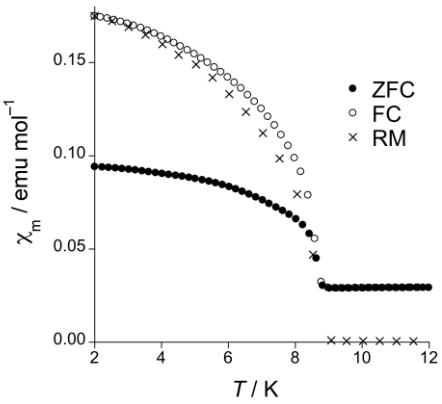

Figure 9: ZFC, FC (applied magnetic field 25 Oe) and remnant magnetization for compound **5**, showing the appearance of spontaneous magnetization.

The field dependence of the magnetization (Figure S6) shows a fast increment up to 0.2 T, and a linear behavior as the magnetic field is further increased. No significant differences were found in the 2-70 K temperature range. *M* barely reaches 1 μ_B at 7 T and 2 K, far away from the 9 μ_B expected for parallel spin alignment, confirming dominant AF interactions. As temperature is increased, *M* shows identical behavior at the low field range, but a higher slope at higher fields to reach higher magnetization values. All these data confirm again the dominant antiferromagnetic interactions. No hysteresis appears for this compound, which behaves as a very soft magnet.

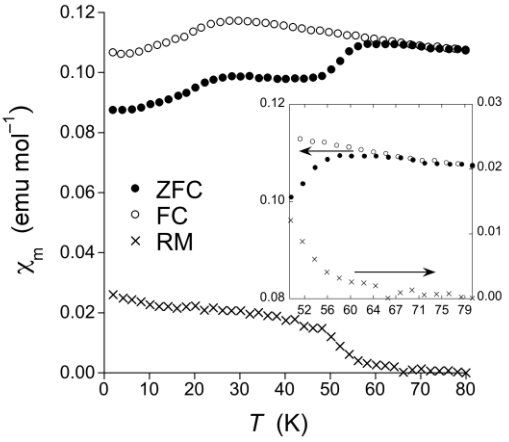

Figure 10: ZFC, FC (applied field 25 Oe) and remnant magnetization (RM) for compound **6**, showing the appearance of spontaneous magnetization. (inset) Detail of the temperature range where ZFC and FC diverge, and when RM disappears.

Discussion

The combination of oxalate, 1,2,4-triazolate and fluoride anions with divalent first row metal cations under hydrothermal conditions has demonstrated to be a versatile reaction. The outcome depends on the nature of the transition metal. Using metal oxalates as starting materials, Mn^{2+} only forms one insoluble phase (**5**) that includes all three ligands in its structure. On the other hand, Co^{2+} and Ni^{2+} (**2** and **3**) only yield a completely different phase where the fluoride anion is not incorporated, no matter the reaction conditions. Zn^{2+} reactivity follows this last reaction pattern although it yields a different polymeric arrangement (**4**). Finally, Fe^{2+} shows an intermediate situation. A fluoride-less compound is the main phase (**1**), but a fluoride-containing product is also obtained (**6**), structurally reminiscent of the Mn^{2+} derivative.

It is interesting to note how the growth of phase **1** and phase **6** follows an opposite building model. **1** is dominated by the coordination mode of the 1,2,4-triazolate units. The 1D triply-bridged chains are stabilized by M_2(ox) dimers, where the oxalate moieties appear with the classic μ_2-bis-chelating mode. On the contrary, the crystal structure of **6** is dominated by the coordination μ_6-mode of the oxalate dianions, which imposes a planar arrangement of metal centers, with the trz moieties acting as ancillary ligands interconnecting the layers.

The origin for this different behavior should be related to the size of the metal cations. Larger dications, such as Mn^{2+}, can accommodate the μ_6-mode, which requires longer bonding distances. Indeed, **5** includes heptacoordinated metal centers, where the larger atomic radii of Mn^{2+} allows the stabilization of μ_3-F bridges. Co^{2+}, Ni^{2+} and Zn^{2+} are too small to stabilize this multiple bonding, preferring the formation of the chain structure. Fe^{2+} is an intermediate case, where both structural types are stable, even in the absence of the μ_3-F bridges.

This series shows how different structural features result in completely different magnetic behavior. The compounds dominated by the M-trz-M and M-ox-M connectivity (**1**, **2** and **3**) exhibit paramagnetic behavior in all the temperature range studied, with significant antiferromagnetic interactions between spin carriers, stabilizing a non-magnetic ground state due to the 1D plus dimer magnetic connectivity. In general,

AF interactions are significantly stronger through the oxalate bridge.

Compounds **5** and **6** include multiple triangular arrays of AF coupled paramagnetic centers, favoring the appearance of competing interactions. Both materials exhibit spontaneous magnetization and memory effect appearing at 9 and 66 K, respectively, as demonstrated by the divergence of the corresponding ZFC/FC data along the remnant magnetization. No other physical origin can be reasonably claimed for the observed data. Furthermore, the absence of a frequency dependent ac susceptibility suggests these materials exhibit magnetic ordering. **5** contains μ_3-fluoride and μ_6-oxalate, both of them forming AF triangles. In this case, the Mn–F distances are significantly shorter than the corresponding Mn–oxalate ones, suggesting that the μ_3-fluoride bridge is the major contribution to the magnetic features. On the contrary, the μ_6-oxalate connecting mode in **6** is the only possible origin for competing interactions. Moreover, **6** exhibits the highest T_C reported for oxalate based-magnets (Table 3), and the second highest T_C when compared with molecule-based homometallic magnets (Table 4), only surpassed by an oxo-bridged compound.[53]

Table 3. Ordering temperatures for a selection of oxalate-based magnets.

network	order	T_C (K)	ref
$[Fe^{II}_3(trz)_2(ox)F_2]$ (**6**)	WF	66	this work
$[Fe^{II}Fe^{III}(ox)_3]^-$	ferri	48	54
$[Fe^{II}Fe^{III}(ox)_3]^-$	ferri	45	55
$[Mn^{II}Fe^{III}(ox)_3]^-$	WF	31	56
$[Mn^{II}Fe^{III}(ox)_3]^-$	WF	29	57
$[Mn^{II}Fe^{III}(ox)_3]^-$	WF	27	58
$[Fe^{II}_3(H_2O)_4\{Fe^{III}(ox)_3\}_3]^{3-}$	ferri	26	59
$[Fe(ox)(CH_3OH)]$	WF	23	60
$[Fe^{II}Mn^{III}(ox)_3]^-$	WF	21	61
$[Ni^{II}Mn^{III}(ox)_3]^-$	ferri	21	61
$[Mn^{II}Fe^{III}(ox)_3]^-$	WF	20	62
$[Mn^{II}_3(H_2O)_4\{Fe^{III}(ox)_3\}_3]^{3-}$	WF	14	62
$[NiCr(ox)_3]^-$	ferro	14	63
$[Co^{II}_2(ox)_3]^{2-}$	WF	9	64
$[Mn_3(trz)_2(ox)F_2]$ (**5**)	WF	9	this work
$[MnCr(ox)_3]^-$	ferro	6	63
$[Mn(CH_3OH)Cr(ox)_3]^{2-}$	ferri	5	65

ferro = ferromagnetic; ferri = ferrimagnetic; WF = weak ferromagnet.

Table 4. Ordering temperatures for a selection of molecule-based weak ferromagnets.

network	linker	S	T_C (K)	ref
$(Et\text{-}NH_3)_2[Fe_2O(ox)_2Cl_2]$	oxo	5/2	70.0	53
$[Fe_3(trz)_2(ox)F_2]$ (**6**)	oxalate	2	66.0	this work
$Cr(dca)_2$	dca	2	47.0	66
$Co(2\text{-}pymS)_2$	pm	3/2	42.0	67
$Na_3[Mn_3(HCOO)_9]$	oxo	5/2	40.0	68
$(NH_4)_2[Fe_2O(ox)_2Cl_2]$	oxo	5/2	40.0	69
$[NH_2(CH_3)_2]Ni(CHOO)_3$	carboxy	1	35.6	70
$Mn(4\text{-}PMK)(N_3)_2$	azide	5/2	22.0	71
$Fe[C_6H_5PO_4]$	phos	5/2	21.5	72
$Mn(2\text{-}pymS)_2$	pm	5/2	21.2	67
$Ni(mtpo)_2(H_2O)$	pm	1	19.0	73
$Fe_3(imid)_6(imidH)_2$	imidazole	2	17.0	74
$[dmenH][Co_2(HCOO)_6]$	carboxy	3/2	16.7	75
$Co(N_3)_2(ampyz)$ (3D)	azide	3/2	16.0	76
$Mn(dca)_2$	dca	5/2	15.9	77
$Co_2(pmtz)_4$	tetrazole	3/2	15.0	78
$[NH_2(CH_3)_2]Co(CHOO)_3$	carboxy	3/2	14.9	75
Co(bIM)(acetate)	imidazole	3/2	13.0	79
$Mn_2(PMA)(N_3)_4$	azide	5/2	12.5	80
$Co_4(OMe)_2(O_2CPh)_2(dhq)_2$	alcoxo	3/2	12.0	81
$Co(N_3)_2(4acpy)_2$	azide	3/2	11.2	82
$Co(N_3)_2(ampyz)$ (2D)	azide	3/2	10.0	82
$Co(dca)_2$	dca	3/2	9.0	83
$[Mn_3(trz)_2(ox)F_2]$ (**5**)	oxalate	5/2	9.0	this work
$[dmenH][Mn_2(HCOO)_6]$	carboxy	5/2	8.5	78
$[NH_2(CH_3)_2]Mn(HCOO)_3$	carboxy	5/2	8.5	73
$Mn(dca)_2(H_2O)$	dca	5/2	6.3	84
$Co_2(TDDC)_2(H_2O)_2$	carboxy	3/2	6.0	85
$[Fe(dca)_2]_2(pm)$	dca	2	5.6	86
$Co_4(pico)_4(4,4'\text{-}bpy)_3(H_2O)_2$	carboxy	3/2	3.0	87
$Co(mtpo)_2(H_2O)$	pm	3/2	3.0	75
$Mn(btr)_2$	triazole	5/2	2.6	88

acpy = 4-acetylpyridine; ampyz = 2-aminopyrazine; bIM = benzimidazole; 4,4'-bpy = 4,4'-bipyridyl; carboxy = carboxylate; dca = dicyanamide; dmen = *N*,*N*‘-dimethylethylenediamine; Hbtr = 3,4'-bi-1,2,4-triazole; Hmtpo = 5-methyl-1,2,4-triazolo[1,5-a]pyrimidin-7(4H)-one; phos = phosphate; pico = 3-hydroxypicolinate; pm = pyrimidine; 4-PMK = 4-pyridylmethylketazine; pmtz = 5-(pyrimidyl) tetrazolate; 2-pymSH = 2-Mercaptopyrimidine; TDDC = 2,1,3-thiadiazole-4,5-dicarboxylate.

CONCLUSIONS

Mixing of two short-pathway connecting organic ligands, oxalate and 1,2,4-triazolate, in the synthesis of coordination polymers has lead to the isolation of 3D networks with strong dominant antiferromagnetic super-exchange interactions. The geometry of **1-3** is dominated by the formation of 1D μ_3-triazole chains interleaved by oxalate-bridged dimers, where the oxalate anion acts in its classic μ_2-bis-chelating coordination mode. Introduction of fluoride anions yields different coordination polymers for the larger metal dications (Mn, **5** and Fe, **6**), whose structure is dominated by the formation of corrugated 2D layers containing the μ_6-oxalate

connectivity. These are the first compounds where the oxalate ligand connects six paramagnetic centers.

It is worth noting the success of this mixed-ligand homometallic strategy to induce complex magnetic structures. In this case, fluoride anions have allowed, for the first time, the identification of a μ_6-oxalate bridge, a connectivity expected to stabilize magnetic ground states in homometallic compounds due to the appearance of competing interactions. This is confirmed by the spontaneous magnetization observed in both compounds.

6 exhibits the highest ordering temperature for an oxalate-based magnet, when containing Fe^{2+} (S = 2). This illustrates the excellent opportunity offered by the μ_6-oxalate arrangement to reach even higher temperature molecule-based magnets. We can envision higher ordering temperatures in μ_6-oxalate magnetic compounds by the incorporation of highly anisotropic metal centers (Co^{2+}) and/or stronger oxalate-based coupling (Ni^{2+}). However, the smaller size of these cations may need larger counter-anions to stabilize analogous networks. This work is under way.

ASSOCIATED CONTENT

Supporting Information. Additional characterization data, including powder X-ray diffraction and additional magnetic data. This material is available free of charge via the Internet at http://pubs.acs.org.

AUTHOR INFORMATION

Corresponding Author

*jrgalan@iciq.es

ACKNOWLEDGMENT

We thank the financial support of the EU (ERC Stg grant 279313, CHEMCOMP), the Spanish Ministerio de Economía y Competitividad (MINECO) through Severo Ochoa Excellence Accreditation 2014-2018 (SEV-2013-0319) and the ICIQ Foundation. MNCO gratefully thanks the Marie Curie COFUND Action from the European Commission for co-financing her postdoctoral fellowship.

REFERENCES

(1) Bradshaw, D.; Claridge, J. B.; Cussen, E. J.; Prior, T. J.; Rosseinsky, M. J. *Acc. Chem. Res.* **2005,** *38*, 273–282.

(2) Evangelisti, M.; Luis, F.; de Jongh, L. J.; Affronte, M. *J. Mater. Chem.* **2006,** *16*, 2534–2549.

(3) Coronado, E.; Galán-Mascarós, J. R. *J. Mater. Chem.* **2005,** *15*, 66–74.

(4) Gütlich, P.; Garcia, Y.; Woike, T. *Coord. Chem. Rev.* **2001,** *219*, 839–879.

(5) Mercuri, M. L.; Deplano, P.; Pilia, L.; Serpe, A.; Artizzu, F. *Coord. Chem. Rev.* **2010,** *254*, 1419–1433.

(6) Miller, J. S. *Chem. Soc. Rev.* **2011,** *40*, 3266–3296.

(7) Verdaguer, M.; Bleuzen, A.; Marvaud, V.; Vaissermann, J.; Seuleiman, M.; Desplanches, C.; Scuiller, A.; Train, C.; Garde, R.; Gelly, G.; Lomenech, C.; Rosenman, I.; Veillet, P.; Cartier, C.; Villain, F. *Coord. Chem. Rev.* **1999,** *190–192*, 1023–1047.

(8) Ruiz, E.; Rodríguez-Fortea, A.; Alvarez, S.; Verdaguer, M. *Chem. Eur. J.* **2005,** *11*, 2135–2144.

(9) Holmes, S. M.; Girolami, G. S. *J. Am. Chem. Soc.* **1999,** *121*, 5593–5594.

(10) Bozdag, K. D.; Yoo, J. W.; Raju, N. P.; McConnell, A. C.; Miller, J. S.; Epstein, A. J. *Phys. Rev. B* **2010,** *82*, 094449.

(11) Coronado, E.; Galán-Mascarós, J. R.; Gómez-García, C. J.; Martínez-Agudo, J. M. *Adv. Mater.* **1999,** *11*, 558–561.

(12) Huang, Z. L.; Drillon, M.; Masciocchi, N.; Sironi, A.; Zhao, J. T.; Rabu, P.; Panissod, P. *Chem. Mater.* **2000,** *12*, 2805–2812.

(13) Rogez, G.; Massobrio, C.; Rabu, P.; Drillon, M. *Chem. Soc. Rev.* **2011,** *40*, 1031–1058.

(14) Miller, J. S.; Manson, J. L. *Acc. Chem. Rev.* **2001,** *34*, 563–570.

(15) Kaneko, W.; Kitagawa, S.; Ohba, M. *J. Am. Chem. Soc.* **2007,** *129*, 248–249.

(16) Sieklucka, B.; Podgajny, R.; Korzeniak, T.; Nowicka, B.; Pinkowicz, D.; Koziel, M. *Eur. J. Inorg. Chem.* **2011,** 305–326.

(17) Her, J. H.; Stephens, P. W.; Kareis, C. M.; Moore, J. G.; Miller, J. S. *Angew. Chem. Int. Ed.* **2010,** *49*, 7773–7775.

(18) Kaye, S. S.; Choi, H. J.; Long, J. R. *J. Am. Chem. Soc.* **2008,** *130*, 16921–16925.

(19) Zheng, Y. Z.; Zheng, Z.; Chen, X. M. *Coord. Chem. Rev.* **2014,** *258*, 1–15.

(20) Gruselle, M.; Train, C.; Boubekeur, K.; Gredin, P.; Ovanesyan, N. *Coord. Chem. Rev.* **2006,** *250*, 2491–2500.

(21) Train, C.; Gheorghe, R.; Krstic, V.; Chamoreau, L. M.; Ovanesyan, N. S.; Rikken, G. L. J. A.; Gruselle, M.; Verdaguer, M. *Nat. Mater.* **2008,** *7*, 729–734.

(22) Coronado, E.; Galán-Mascarós, J. R.; Gómez-García, C. J.; Martínez-Agudo, J. M.; Martínez-Ferrero, E.; Waerenborgh, J. C.; Almeida, M. *J. Solid State Chem.* **2001,** *159*, 391–402.

(23) Hernandez-Molina, M.; Lorenzo-Luis, P. A.; Ruiz-Perez, C. *CrystEngComm* **2001**, *16*, 60–63.

(24) Pardo, E.; Train, C.; Liu, H.; Chamoreau, L. M.; Dhkil, B.; Boubekeur, K.; Lloret, F.; Nakatani, K.; Tokoro, H.; Ohkoshi, S. I.; Verdaguer, M. *Angew. Chem. Int. Ed.* **2012,** *51*, 8356–8360.

(25) Zhang, B.; Zhang, Y.; Wang, Z.; Wang, D.; Baker, P. J.; Pratt, F. L.; Zhu, D. *Sci. Rep.* **2014,** *4*, 6451.

(26) Escuer, A.; Esteban, J.; Perlepes, S. P.; Stamatatos, T. C. *Coord. Chem. Rev.* **2014,** *275*, 87–129.

(27) Ribas, J.; Escuer, A.; Monfort, M.; Vicente, R.; Cortés, R.; Lezama, L.; Rojo, T. *Coord. Chem. Rev.* **1999,** *193-195*, 1027–1068.

(28) Escuer, A.; Aromí, G. *Eur. J. Inorg. Chem.* **2006,** 4721–4736.

(29) Li, R. Y.; Wang, B. W.; Wang, X. Y.; Wang, X. T.; Wang, Z. M.; Gao, S. *Inorg. Chem.* **2009,** *48*, 7174–7180.

(30) Manson, J. L.; Huang, Q. Z.; Lynn, J. W.; Koo, H. J.; Whangbo, M. H.; Bateman, R.; Otsuka, T.; Wada, N.; Argyriou, D. N.; Miller, J. S. *J. Am. Chem. Soc.* **2001,** *123*, 162–172.

(31) Miyasaka, H.; Nakata, K.; Sugiura, K. I.; Yamashita, M.; Clérac, R. *Angew. Chem. Int. Ed.* **2004,** *43*, 707–711.

(32) Miyasaka, H.; Nakata, K.; Lecren, L.; Coulon, C.; Nakazawa, Y.; Fujisaki, T.; Sugiura, K. I.; Yamashita, M.; Clérac, R. *J. Am. Chem. Soc.* **2006**, *128*, 3770–3783.

(33) Manson, J. L.; Schlueter, J. A.; Nygren, C. L. *Dalton Trans.* **2007,** 646–652.

(34) Batten, S. R.; Murray, K. S.; *Coord. Chem. Rev.* **2003,** *246*, 103–130.

(35) Clérac, R.; O'Kane, S.; Cowen, J.; Ouyang, X.; Heintz, R.; Zhao, H.; Bazile, M. J.; Dunbar, K. R. *Chem. Mater.* **2003,** *15*, 1840–1850.

(36) Deumal, M.; Rawson, J. M.; Goeta, A. E.; Howard, J. A. K.; Copley, R. C. B.; Robb, M. A.; Novoa, J. J. *Chem. Eur. J.* **2010,** *16*, 2741–2750

(37) Fujita, W.; Kikuhi, K. *Chem. Asian J.* **2009,** *4*, 400-405.

(38) Rabu, P.; Drillon, M. *Adv. Eng. Mater.* **2003,** *5*, 189–210.

(39) Weng, D. F.; Wang, Z. M.; Gao, S. *Chem. Soc. Rev.* **2011**, *40*, 3157–3181.

(40) Ramirez, A. P. *MRS Bull.* **2005,** *30*, 447–451.

(41) Baker, M. L.; Timco, G. A.; Piligkos, S.; Mathieson, J. S.; Mutka, H.; Tuna, F.; Kozłowski, P.; Antkowiak, M.; Guidi, T.; Gupta, T.; Rath, H.; Woolfson, R. J.; Kamieniarz, G.; Pritchard, R. G.; Weihe, H.; Cronin, L.; Rajaraman, G.; Collison, D.; McInnes, E. J. L.; Winpenny, R. E. P. *Proc. Natl. Acad. Sci. U.S.A.* **2012,** *109*, 19113-19118.

(42) Hatnean, J. A.; Raturi, R.; Lefebvre, J.; Leznoff, D. B.; Lawes, G.; Johnson, S. A. *J. Am. Chem. Soc.* **2006,** *128*, 14992–14999.
(43) Wöhlert, S.; Tomkowicz, Z.; Rams, M.; Ebbinghaus, S. G.; Fink, L.; Schmidt, M. U.; Näther, C. *Inorg. Chem.* **2014**, *53*, 8298–8310.
(44) Tsai, J. D.; Yang, C. I. *Danton Trans.* **2014,** *43*, 15576–15582.
(45) Shores, M. P.; Bartlett, B. M.; Nocera, D. G. *J. Am. Chem. Soc.* **2005,** *127*, 17986–17987.
(46) Burla, M. C.; Caliandro, R.; Camalli, M.; Carrozzini, B.; Cascarano, G. L.; Giacovazzo, C.; Mallamo, M.; Mazzone, A.; Polidori, G.; Spagna, R. *J. Appl. Crystallogr.* **2012,** *45*, 357-361.
(47) Sheldrick, G. M. *Acta Crystallogr.* **2008,** *A64*, 112–122.
(48) Grosjean, A.; Négrier, P.; Bordet, P.; Etrillard, C.; Mondieig, D.; Pechev, S.; Lebraud, E.; Letard, J. F.; Guionneau, P. *Eur. J. Inorg. Chem.* **2013**, 796–802.
(49) Fisher, M. E. *Am. J. Phys.* **1964,** *32*, 343–346.
(50) Meyer, A.; Gleizes, A.; Girerd, J. J.; Verdaguer, M.; Kahn, O. *Inorg. Chem.* **1982,** *21*, 1729–1739.
(51) Glerup, J.; Goodson, P. A.; Hodgson, D. J.; Michelsen, K. *Inorg. Chem.* **1995**, *34*, 6255–6264.
(52) Bellouard, F.; Clemente-Leon, M.; Coronado, E.; Galan-Mascaros, J. R.; Gomez-Garcia, C.; Romero, F. M.; Dunbar, K. R. *Eur. J. Inorg. Chem.*, 1603–1606.
(53) Armentano, D.; De Munno, G.; Mastropietro, T. F.; Julve, M.; Lloret, F. *J. Am. Chem. Soc.* **2005,** *127*, 10778–10779.
(54) Mathonière, C.; Nuttall, C. J.; Carling, S. G.; Day, P. *Inorg. Chem.* **1996**, *35*, 1201–1206.
(55) Mathonière, C.; Carling, S. G.; Yusheng, D.; Day, P. *J. Chem. Soc., Chem. Commun*. **1994**, 1551–1552**.**
(56) Clemente-León, M.; Coronado, E.; Gómez-García, C. J.; Soriano-Portillo, A. *Inorg. Chem.* **2006**, *45*, 5653–5660.
(57) Ovanesyan, N. S.; Makhaev, V. D.; Aldoshin, S. M.; Gredin, P.; Boubekeur, K.; Train, C.; Gruselle, M. *Dalton Trans.* **2005,** 3101–3107.
(58) Carling, S. G.; Mathonière, C.; Day, P.; Malik, K. M. A.; Coles, S. J.; Hursthouse, M. B. *J. Chem. Soc., Dalton Trans.* **1996,** 1839–1843.
(59) Coronado, E.; Galán-Mascarós, J. R.; Martí-Gastaldo, C.; Waerenborgh, J. C.; Gaczyński, P. *Inorg. Chem.* **2008**, *47*, 6829–6839.
(60) Zhang, B.; Zhang, Y.; Zhang, J.; Li, J. C.; Zhu, D. *Dalton Trans.* **2008**, 5037–5040.
(61) Coronado, E.; Galán-Mascarós, J. R.; Martí-Gastaldo, C. *J. Mater. Chem.* **2006**, *16*, 2685–2689.
(62) Coronado, E.; Galán-Mascarós, J. R.; Gómez-García, C. J.; Martínez-Ferrero, E.; Almeida, M.; Waerenborgh, J. C. *Eur. J. Inorg. Chem.* **2005**, 2064–2070.
(63) Tamaki, H.; Zhong, Z. J.; Matsumoto, N.; Kida, S.; Koikawa, M.; Achiwa, N.; Hashimoto, Y.; Okawa, H. *J. Am. Chem. Soc.* **1992,** *114*, 6974–6979.
(64) Hernández-Molina, M.; Lloret, F.; Ruiz-Pérez, C.; Julve, M. *Inorg. Chem.* **1998**, *37*, 4131–4135.
(65) Coronado, E.; Galán-Mascarós, J. R.; Martí-Gastaldo, C.; Murcia-Martínez, A. *Dalton Trans.* **2006**, 3294–3299.
(66) Manson, J. L.; Kmety, C. R.; Epstein, A. J.; Miller, J. S. *Inorg. Chem.* **1999**, *38*, 2552–2553.
(67) Zhang, J.; Gao, S.; Zhang, X. X.; Wang, Z. M.; Che, C. M. *Dalton Trans.* **2012,** *41*, 2626–2631.
(68) Paredes-García, V.; Vega, A.; Novak, M. A.; Vaz, M. G. F.; Souza, D. A.; Venegas-Yazigi, D.; Spodine, E. *Inorg. Chem.* **2009,** *48*, 4737–4742.
(69) Armentano, D.; Mastropietro, T. F.; De Munno, G.; Rossi, P.; Lloret, F.; Julve, M. *Inorg. chem.* **2008,** *47*, 3772–3786.
(70) Wang, X. Y.; Gan, L.; Zhang, S. W.; Gao, S. *Inorg. Chem.* **2004,** *43*, 4615–4625.
(71) Gao, E. Q.; Wang, Z. M.; Yan, C. H. *Chem. Commun.* **2003,** 1748–1749.
(72) Bellito, C.; Federici, F.; Altomare, A.; Rizzi, R.; Ibrahim, S. A. *Inorg. Chem.* **2000,** *39*, 1803–1808.
(73) Lin, Q. P.; Zhang, J.; Cao, X. Y.; Yao, Y. G.; Li, Z. J.; Zhang, L.; Zhou, Z. F. *CrystEngComm* **2010,** *12*, 2938–2942.
(74) Retting, S. J.; Storr, A.; Summers, D. A.; Thompson, R. C.; Trotter, J. *J. Am. Chem. Soc.* **1997,** *119*, 8675–8680.
(75) Wang, Z.; Zhang, X.; Batten, S. R.; Kurmoo, M.; Gao, S. *Inorg. Chem.* **2007,** *46*, 8439–8441.
(76) Boonmak, J.; Nakano, M.; Chaichit, N.; Pakawatchai, C.; Youngme, S. *Inorg. Chem.* **2011,** *50*, 7324–7333.
(77) Manson, J. L.; Kmety, C. R.; Palacio, F.; Epstein, A. J.; Miller, J. S. *Chem. Mater.* **2001,** *13*, 1068–1073.
(78) Rodríguez-Diéguez, A.; Palacios, M. A.; Sironi, A.; Colacio, E. *Dalton Trans.* **2008,** *21*, 2887–2893.
(79) Arai, L.; Nadeem, M. A.; Bhadbhade, M.; Stride, J. A. *Dalton Trans.* **2010,** *39*, 3372–3374.
(80) Gao, E. Q.; Bai, S. Q.; Wang, Z. M.; Yan, C. H. *J. Am. Chem. Soc.* **2003,** *125*, 4984–4985.
(81) Yang, C. I.; Chuang, P. H.; Lee, G. H.; Peng, S. M.; Lu, K. L. *Inorg. Chem.* **2012,** *51*, 757–759.
(82) Wang, X. Y.; Wang, Z. M.; Gao, S.; *Inorg. Chem.* **2008,** *47*, 5720–5726.
(83) Jensen, P.; Batten, S. R.; Fallon, G. D.; Moubaraki, B.; K. S. Murray. D. J. Price, *Chem. Commun.* **1999**, 177–178.
(84) Jensen, P.; Price, D. J.; Batten, S. R.; Moubaraki, B.; Murray, K. S. *Chem. Eur. J.* **2000,** *6*, 3186–3195.
(85) Li, J. R.; Yu, Q.; Tao, Y.; Bu, X. H.; Ribas, J.; Batten, S. R. *Chem. Commun.* **2007**, 2290–2292.
(86) Takagami, N.; Ishida, T.; Nogami, T. *Bull. Chem. Soc. Jpn.* **2004**, *77*, 1125–1134.
(87) Zeng, M. H.; Zhang, W. X.; Sun, X. Z.; Chen, X. M. *Angew. Chem. Int. Ed.* **2005**, *44*, 3079–3082.
(88) Jia, L. H.; Liu, A. C.; Wang, B. W.; Wang, Z. M.; Gao, S. *Polyhedron* **2011**, *30*, 3112–3115.

TOC entry:

Oxalate-based magnets: Four oxalate-based coordination polymers were obtained: $[M_2(H_2O)(\mu_2\text{-}ox)][M_2(\mu_3\text{-}trz)_6]$ (M = Fe, Co, Ni), $[Zn_2(H_2O)(\mu_3\text{-}trz)_2(\mu_2\text{-}ox)]$, $[Mn_3(\mu_3\text{-}trz)_2(\mu_6\text{-}ox)(\mu_3\text{-}F)_2]$ and $[Fe_3(\mu_3\text{-}trz)_2(\mu_6\text{-}ox)(\mu_2\text{-}F)_2]$. The two last derivatives present the novel magnetic μ_6-oxalate connectivity, which promotes competing interactions in these antiferromagnetic networks, exhibiting spontaneous magnetization at temperatures as high as 66 K.